Harnessing Long-Range Temporal Correlations for Advanced Epilepsy Classification

Vadim V. Grubov [ORCID],[1] Alexander K. Kuc [ORCID],[1] Semen A. Kurkin [ORCID],[1] Denis A. Andrikov,[2] Nikita Utyashev [ORCID],[3] Vladimir A. Maksimenko,[4] Oleg E. Karpov,[3] and Alexander E. Hramov [ORCID][1]

[1]*Baltic Center for Neurotechnology and Artificial Intelligence, Immanuel Kant Baltic Federal University, 236041 Kaliningrad, Russia*
[2]*Bauman Moscow State Technical University, 105005 Moscow, Russia*
[3]*Federal State Budgetary Institution "National Medical and Surgical Center named after N.I. Pirogov"*
of the Ministry of Health of the Russian Federation, 127051 Moscow, Russia
[4]*Neuromorphic Computing Center, Neimark University, 603081 Nizhny Novgorod, Russia*

In this study, we suggest that detrended fluctuation analysis may reveal alternations in long-range temporal correlations associated with epileptic status. We consider two groups of subjects: patients with confirmed focal epilepsy, and healthy controls. Both groups were exposed to intermittent photic stimulation. Analysis based on event-related spectral perturbations revealed that photic driving in epileptic patients is higher in the α band and lower in other bands. This result is related to altered excitability in nonphotosensitive epilepsy. To prove this, we tested two hypotheses. First, we assess long-range temporal correlations using detrended fluctuation analysis, with the objective of evaluating whether this metric differs between epileptic patients and healthy controls through the application of between-subject statistics. Second, we investigate whether detrended fluctuation analysis provides more valuable insights into the aforementioned differences in comparison to traditional spectral analysis of brain signals. More precisely, we test if a machine learning algorithm trained on detrended fluctuation analysis-based features outperforms one trained on the spectral-based features in classifying between epileptic patients and controls. Furthermore, we study whether the features differ between classifiers by implementing feature importance assessment. Our findings demonstrate that the classifier based on detrended fluctuation analysis exhibits higher efficiency, and its features are notably distinct from those of the classifier based on spectral analysis. We postulate that the long-range temporal correlations captured via detrended fluctuation analysis reveal novel aspects of the epileptic brain response to intermittent photic stimulation, and they are more pronounced than the features captured via spectral analysis.

I. INTRODUCTION

A. Problem overview

The spontaneous neural oscillations of the brain are known for pronounced variability in amplitude, duration, frequency, and recurrence. The major unresolved question is whether fluctuations in these oscillations reflect a memory of the dynamics of the system for more than a few seconds [1]. This leads to a great interest in studying long-term spatiotemporal patterns in the brain, which can be expressed through long-range temporal correlations (LRTCs) [2].

A common way to analyze scaling behavior in time series and quantify LRTC is detrended fluctuation analysis (DFA), which incorporates less strict assumptions about the stationarity of the signal than the autocorrelation function [3]. DFA can capture features of brain activity distinct from those revealed by traditional spectral analysis [4], which offers a unique perspective on neural oscillations research.

The salient features of DFA become particularly significant in the investigation of certain complex and poorly defined brain states. A prime example of this is the brain response to intermittent photic stimulation (IPS) [5], a widely employed technique in the clinical diagnosis of epilepsy [6]. The diagnosis is based on the response specific to the epileptic brain.

It is assumed that epileptic status is tied to increased cortex excitability due to the loss of inhibitory control [7]. At the same time, the dominant hypothesis of LRTC in neural oscillations suggests that excitatory-inhibitory balance plays a crucial role, and its disruption may lead to dysfunction [8]. In this context, DFA may reflect epilepsy-related changes in LRTC and provide new insights into differences in neural activations during IPS between epileptic patients and healthy controls.

B. Long-range temporal correlations and detrended fluctuation analysis

In recent years, LRTC was extensively used in analysis of neuronal signals [9–11], however there are certain fundamental issues waiting to be addressed. Findings prove that the brain operates on a wide range of timescales, varying from milliseconds in stimulus perception to tens of seconds during extensive cognitive load [12]. This leads to the suggestion that

neural activity in the brain can exhibit scale-free dynamics, i.e., dynamics without characteristic scales [13]. More importantly, this type of dynamics turned out to be crucial for physiological functions of the brain in both normal and pathological states [14–16]. However, neuronal dynamics are rarely studied with approaches incorporating different timescales in order to better understand integrative brain mechanisms [4]. In this sense, LRTC provides a unique opportunity to study how neuronal activity unfolds in time with respect to different timescales.

LRTCs were first discovered in electroencephalogram (EEG) and magnetoencephalogram (MEG) signals during periods of eyes-closed and eyes-open rest [2]. These initial findings, demonstrating LRTC in α and β oscillations within timescales of 5–300 s, were subsequently confirmed in shorter experiments and a more restricted range of 1–25 s [9,17,18]. LRTCs have also been observed in θ and δ frequency bands [18,19], although they are less commonly found in higher frequencies [20]. Certain studies indicate that LRTCs are influenced by low-level biological factors, such as genetics, rather than random experimental variables [17]. This finding contributes to the test-retest reliability of DFA. Furthermore, DFA exponents have been shown to be independent of the power of neuronal oscillations in both scalp [17,18] and subdural EEG [19], further reinforcing the robustness of this analytical approach.

C. Intermittent photic stimulation and photic driving

Diagnostics with IPS relies heavily on the detection of an abnormal EEG trait known as the photoparoxysmal response (PPR) [21]. However, PPR is observed exclusively in photosensitive epilepsy, which accounts for only 2–5% of all epilepsy cases, potentially limiting the diagnostic utility of IPS [22]. Another type of response to IPS is photic driving (PD), characterized by steady-state visual evoked potentials (SSVEPs) at the frequency and/or harmonics of the IPS. Findings indicate that PD might differentiate between controls and individuals with neurological disorders, including epilepsy [23–25]. PD is commonly investigated using spectral analysis techniques, such as the continuous wavelet transform (CWT) [26]. Various scoring characteristics have been introduced to evaluate the manifestation of PD and identify differences between patients and controls [26,27], however there is no consensus regarding the diagnostic utility of PD. As a result, the efficacy of IPS for diagnosing nonphotosensitive epilepsy remains a topic of ongoing debate.

D. Machine learning and domain knowledge

ML is frequently associated with classification tasks, and a burgeoning trend is the integration of ML with domain knowledge [28,29]. The underlying principle is that ML has the potential to detect subtle data properties that often elude human observation and conventional data analysis methods, while domain knowledge, often derived from statistical testing, provides fundamental insights into data features that have been thoroughly investigated through scientifically rigorous research but may be underrepresented in a specific dataset. Combining these two approaches offers clear advantages. For example, integrating the results of traditional statistical tests with significant features from the ML-based classifier can ensure a more robust identification of biomarkers in EEG [30,31]. While many ML-based classifiers operate as "black boxes" with difficult-to-interpret features, there is increasing interest in assessing feature importance, which can potentially enhance the interpretability of such classifiers [32,33]. Increasing the interpretability of machine learning methods and utilizing explainable AI (XAI) techniques is particularly relevant in biomedical tasks [34–36].

E. Contribution of the study

This study contributes by testing two hypotheses. First, we assess LRTC using DFA and evaluate whether this metric differs between epileptic patients and healthy controls using between-subject statistics. Second, we investigate whether DFA provides more valuable insights into the aforementioned differences compared to traditional spectral analysis of brain signals. More precisely, we test if the machine learning algorithm trained on the DFA-based features outperforms the algorithm trained on the spectral-based features in classifying between epileptic patients and controls. Additionally, we test whether DFA-based features differ from spectral-based features by implementing feature importance assessment.

The structure of the study is presented in Fig. 1. First, we consider a clinical dataset consisting of raw EEG signals from control subjects and patients with focal epilepsy. We perform basic preprocessing, including band-pass and notch filtering, as well as artifact removal based on independent component analysis. Detailed information regarding this step is provided in Sec. II B.

Second, data are processed using two distinct approaches: CWT and DFA. This processing is performed for each IPS frequency across five frequency ranges and 25 EEG channels. This step yields two characteristics: wavelet power (w) and DFA scaling factor (μ). Detailed descriptions of these methods are found in Secs. II C and II D, respectively.

Third, cluster analysis is implemented to identify spatial clusters specific to IPS frequency and frequency range, where w or μ exhibit significant differences between control subjects and patients. Details regarding this step are provided in Sec. II E.

Fourth, the ML approach is applied: two classifiers are trained using the w and μ characteristics, respectively, employing the support vector machine (SVM) method. Each classifier is constructed in two variations: (i) with all features (9 IPS frequencies $\times 5$ frequency ranges $\times 25$ EEG channels) reduced using principal component analysis, and (ii) with features derived from significant clusters. Complete details are presented in Sec. II F. Our findings demonstrate that the efficiency of the DFA-based classifier surpasses that of the CWT-based classifier in both variations.

Fifth, feature importance for classification using both CWT and DFA-based features is assessed with the Boruta method described in Sec. II G. We observe notable differences between features that are significant to both approaches. Specifically, DFA analysis revealed no discernible "resonant" brain response at very low IPS frequencies. However, at higher IPS frequencies, the brain response shifted from the
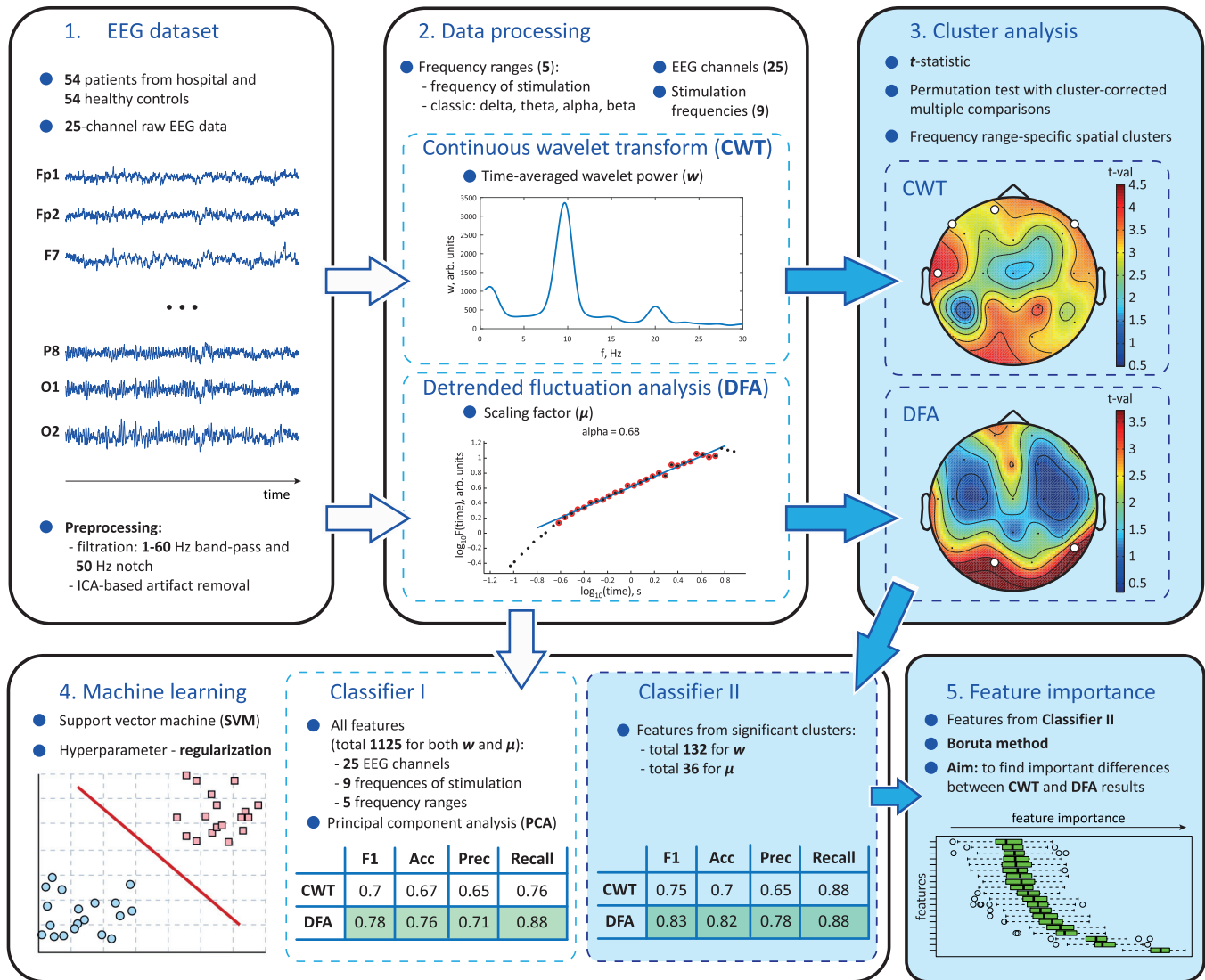
FIG. 1. Structure of the study. Block 1: Clinical dataset with raw EEG signals of controls and patients with focal epilepsy is preprocessed. Subplots here show examples of raw EEG data as well as preprocessing pipeline. Block 2: For data processing, we consider two different approaches: continuous wavelet transform (CWT) and detrended fluctuation analysis (DFA). Corresponding subplots schematically show the results of processing with each method. Block 3: Clustering analysis is used to find spatial clusters with significant difference between controls and patients. Two subplots demonstrate examples of such clusters. Block 4: Results of CWT and DFA are used to train machine learning classifiers with the support vector machine (SVM) method. The subplot here schematically shows the basic principle of SVM. Classifiers are trained in two variants: (i) with all features reduced with principal component analysis, and (ii) with features from significant clusters. Two tables here contain efficiency metrics for both variants of each classifier. Block 5: Feature importance is assessed via the Boruta method to highlight differences between features of CWT and DFA. The subplot here has an example of feature importance ranking.

frontal and temporal areas, as observed in CWT clusters, to parietal and occipital regions. Combining this result with the superior performance of the DFA-based classifier, we posit that LRTCs, assessed through DFA, may reveal novel aspects of brain response to IPS in nonphotosensitive epilepsy.

II. MATERIALS AND METHODS

A. Experimental design

The data for this study were collected at the Pirogov National Medical and Surgical Center (Moscow, Russia). Dataset includes anonymized EEG data of 54 patients of the Center

from 2017 to 2019, and 54 controls recruited from the staff of the Center. Medical procedures were preapproved by the local ethics committee and carried out at the Center following the Helsinki Declaration and medical regulations of the Center. All subjects provided written informed consent before the procedure. For the patients, the sessions of IPS were part of a long-term clinical monitoring aimed at clarifying the diagnosis and specifying the epileptogenic zones. All patients were diagnosed with focal epilepsy, yet the foci were located in different regions (frontal, temporal, parietal) of both hemispheres. Thus, there was no uniformity in the focus placement among the patients. It should be emphasized that the epilepsy was drug-resistant in all patients, so none of the patients were
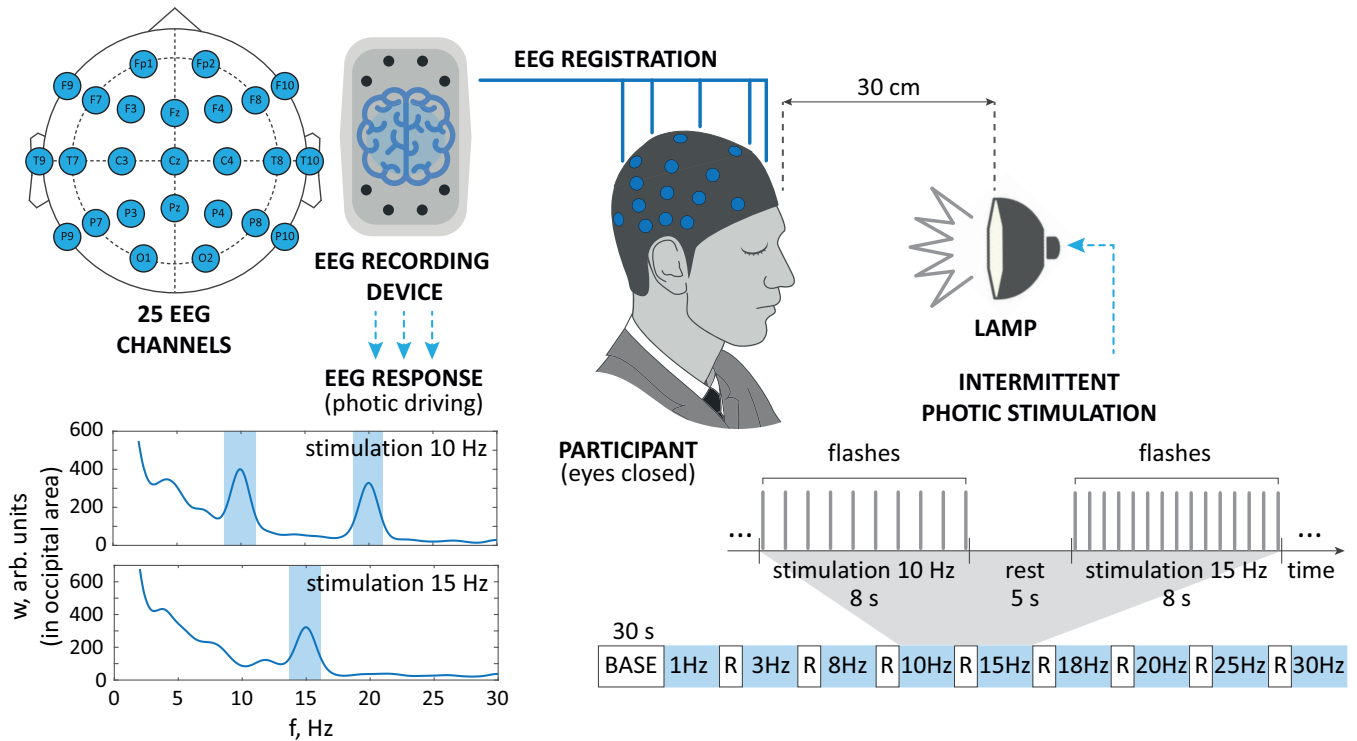
FIG. 2. Experimental setup. Participant sits upright with eyes closed. Intermittent photic stimulation is performed via a lamp with circular reflector. The subplot here illustrates stimulation protocol: 9 frequencies in total with 30-s baseline, stimulation on individual frequencies lasts for 8 s, sessions are separated by 5-s rest. EEG data are collected by a recording device with 25 channels of electrical activity. EEG channel names and locations are shown in the upper left panel. The lower left panel shows the spectra of the typical responses to photic stimulation—photic driving recorded in the occipital cortex (channel O1) at the stimulation frequencies of 10 and 15 Hz.

taking antiepileptic drugs at the time of clinical monitoring. While IPS was employed along hyperventilation to provoke epileptiform activity [37], there was no PPR, so all patients were considered nonphotosensitive. Some patients had more than one session of IPS, but to equalize all subjects we considered only the first session. For the controls, a single session of IPS was recorded under conditions close to clinical.

The experimental setup is shown in Fig. 2. IPS was conducted in a dimly lit room with the participant seated upright and eyes closed. Stimulation was delivered using a lamp equipped with a circular reflector, emitting flashes with an intensity of approximately 0.70 J at a viewing distance of approximately 30 cm. The protocol included stimulation at nine frequencies: $f_{\mathrm{IPS}} = 1, 3, 8, 10, 15, 18, 20, 25$, and 30 Hz. Each stimulation instance lasted for $T_f = 8$ s, followed by a 5-s pause separating stimulation at different frequencies. Prior to IPS, at least 30 s of resting state EEG data were recorded and subsequently used as baseline activity.

B. Data acquisition and preprocessing

"Micromed" encephalograph (Micromed S.p.A., Italy) was used to record EEG signals at a sampling rate of 128 Hz from $C = 25$ EEG channels according to the international "10–20" scheme [38]. A ground electrode was placed on the forehead, and reference electrodes were placed at the ears. Raw EEG is known to be highly susceptible to noise and physiological artifacts, which is especially noticeable in prolonged clinical studies [39]. Certain parasitic components such as

respiration or muscle artifacts have inherent low or high frequency. Therefore, we implemented a band-pass filter (Butterworth 1–60 Hz) to suppress them. An additional 50-Hz notch filter was used to mitigate interference from the power grid. Some other components such as artifacts from blinking and cardiac activity interfere with the common frequency range of EEG (1–40 Hz). To remove such interferences, we used an advanced procedure based on independent component analysis (ICA) [40].

All preprocessing was conducted in MATLAB software using the Fieldtrip toolbox [41].

C. Time-frequency analysis

The spectral power of the EEG was analyzed using continuous wavelet transform (CWT) [42]. The wavelet power (WP) spectrum

$$E^i(f, t) = [W^i(f, t)]^2 \qquad (1)$$

was calculated for each ith EEG channel, $X_i(t)$, over the frequency range $f \in [1, 40]$ Hz, which included all frequency ranges of interest for analysis. The complex-valued wavelet coefficients, $W^c(f, t)$, were calculated as follows:

$$W^i(f, t) = \sqrt{f} \int_{t-4/f}^{t+4f} X_i(t)\varphi^*(f, t)dt, \qquad (2)$$

where $i = 1, \ldots, C$ represents the EEG channel number, and the "*" symbol denotes a complex conjugate. The Morlet wavelet was employed as the mother wavelet function,

$\varphi(f, t)$, which is defined as follows:

$$\varphi(f, t) = \sqrt{f} \pi^{1/4} e^{f \omega_0 f(t - t_0)} e^{f(t - t_0)^2/2}, \qquad (3)$$

where $\omega_0 = 2\pi$ represents the central frequency. As indicated in Ref. [43], the Morlet wavelet is advantageous for analyzing EEG recordings that contain a range of rhythms and oscillatory patterns. A comparison of EEG analysis studies utilizing different mother wavelets [42] reveals that the Morlet wavelet offers a discernible wavelet spectrum and superior overall resolution in the frequency-time domain.

CWT analysis was conducted in MATLAB software using the Fieldtrip toolbox [41].

Intervals of 0.5 s were allocated on each side of the trial to account for boundary effects tied to WP calculation. To isolate the WP associated with the effect of IPS, we computed the event-related spectral perturbations (ERSPs) with baseline correction to the background brain activity prior to the IPS session. The ERSP was calculated by subtracting the baseline from the stimulus and dividing the result by the baseline: ERSP = (Stimulus−Baseline)/Baseline. Subsequently, the ERSPs obtained for each EEG channel were averaged over time,

$$w^i(f) = \int_{t_0}^{t_0 + T_f} E^i(f, t) \, dt, \qquad (4)$$

where t_0 is the stimulation start time, and $T_f = 8\,\text{s}$ is the duration of the stimulation. Typical examples of the ERSP $[w^{O1}(t)]$ recorded during IPS at frequencies of 10 and 15 Hz in the occipital cortex (O1 EEG channel) within the frequency range of 1–30 Hz are presented in the bottom left subplot of Fig. 2. In the former case, both the stimulus frequency and its second harmonic (highlighted in blue) are clearly discernible, whereas in the latter case, only the stimulus frequency (also highlighted in blue) is evident.

Then, we introduced 13 frequency ranges $[f_1, f_2]$ under study, in which we considered the average WP:

$$w^i_{\Delta f} = \frac{1}{f_2 - f_1} \int_{f_1}^{f_2} w^i(f) \, df. \qquad (5)$$

First, we considered standardly introduced four frequency bands on the EEG: δ, θ, α, and β. Second, we considered nine frequency ranges associated with stimulation frequencies f_{IPS}, namely we introduced $[f_{\text{IPS}} - 0.5, f_{\text{IPS}} + 0.5]$ Hz for $f_{\text{IPS}} = 1$ Hz, and $[f_{\text{IPS}} - 1, f_{\text{IPS}} + 1]$ Hz for all f_{IPS} higher than 1 Hz. For more details, see Table I.

When addressing processes at a specific stimulation frequency f_{IPS}, we considered 25×5 values of $w^i_{\Delta f}$, which correspond to 25 EEG channels ($i = 1, \ldots, 25$) and five frequency ranges: four standard frequency bands w^i_δ, w^i_θ, w^i_α, and w^i_β, as well as a frequency band corresponding to the specific stimulation frequency $w^i_{\Delta f_{\text{IPS}}}$.

D. Detrended fluctuation analysis

Detrended fluctuation analysis is a powerful tool for analyzing complex time series, particularly when the objective is to understand the structure of the data across different timescales and identify hidden correlations and trends [44].

TABLE I. The size of the windows in which the filter's influence is negligible for each frequency range under study.

Frequency range	Fitting time window (s)
$[1, 4]$ Hz (δ-range)	2.8–7.6
$[4, 7]$ Hz (θ-range)	0.9–2.8
$[8, 12]$ Hz (α-range)	0.2–5.7
$[13, 30]$ Hz (β-range)	0.07–4.2
$[0.5, 1.5]$ Hz ($f_{\text{IPS}} = 1$ Hz)	4.6–5.1
$[2, 4]$ Hz ($f_{\text{IPS}} = 3$ Hz)	1.3–7.6
$[7, 9]$ Hz ($f_{\text{IPS}} = 8$ Hz)	0.2–7.6
$[9, 11]$ Hz ($f_{\text{IPS}} = 10$ Hz)	0.1–6.9
$[14, 16]$ Hz ($f_{\text{IPS}} = 15$ Hz)	0.09–6.9
$[17, 19]$ Hz ($f_{\text{IPS}} = 18$ Hz)	0.07–7.6
$[19, 21]$ Hz ($f_{\text{IPS}} = 20$ Hz)	0.07–4.6
$[24, 26]$ Hz ($f_{\text{IPS}} = 25$ Hz)	0.07–2.1
$[29, 31]$ Hz ($f_{\text{IPS}} = 30$ Hz)	0.07–1.2

The outcome of DFA is a scaling factor (μ) that characterizes the type of correlations present within the data [3]. For instance, $\mu = 0.5$ indicates the absence of correlations, which is consistent with a random wandering process or white noise; $\mu < 0.5$ indicates an anticorrelated process; $\mu > 0.5$ indicates the presence of long-term correlations, which may be indicative of a stable trend.

As in the case of CWT analysis (see Sec. II C), we considered 13 frequency ranges $[f_1, f_2]$ under study, which correspond to both the 4 standard frequency ranges (δ, θ, α, and β) and the 9 frequency ranges associated with stimulation frequencies f_{IPS}. For each stimulation frequency f_{IPS}, DFA was calculated for each ith EEG channel ($i = 1, \ldots, C$) in each standard frequency range and stimulation frequency range to obtain the 5 scaling factors μ^i_δ, μ^i_θ, μ^i_α, μ^i_β, and $\mu^i_{f_{\text{IPS}}}$, respectively.

The DFA-based analysis of each ith EEG channel signal $X_i(t)$ is comprised of the following steps:

(i) *Filtering the signal $X_i(t)$ in the frequency range $[f_1, f_2]$*. We used a finite impulse response (FIR) filter whose order was set to $2/f_1$ s, where f_1 is the lower frequency of the analyzed frequency range. Thus, we can guarantee that the filter window covers at least two cycles of oscillations with frequency f_1 Hz.

(ii) *Calculating the amplitude envelope using the Hilbert transform*. A Hilbert transform $\hat{X}_i(t)$ is performed on the filtered signal $X_{i, \Delta f}(t)$ to produce a phase-shifted signal [45]:

$$\hat{X}_i(t) = \frac{1}{\pi} \int_{-\infty}^{\infty} \frac{X_{i, \Delta f}(\tau)}{t - \tau} \, d\tau. \qquad (6)$$

Then the analytic signal $Z_i(t)$ is obtained as the sum of the original signal and its Hilbert transform: $Z_i(t) = X_{i, \Delta f}(t) + j\hat{X}_i(t)$, where j is an imaginary unit. The envelope amplitude is defined as the modulus of the analytic signal:

$$A_i(t) = |Z_i(t)| = \sqrt{X_{i, \Delta f}(t)^2 + \hat{X}_i(t)^2}. \qquad (7)$$

(iii) *Constructing cumulative series*. A cumulative series, designated as $Y_i(k)$, is constructed using the envelope

amplitude $A_i(t)$ of length N:

$$Y_i(k) = \sum_{t=1}^{k} [A_i(t) - \bar{A}_i], \qquad (8)$$

where $\bar{A}_i = \frac{1}{N} \sum_{t=1}^{N} A_i(t)$.

(iv) *Dividing the dataset into discrete segments*. The cumulative series is partitioned into $N_s = N/s$ segments of length s, with an overlap of 50%.

(v) *Removing the trend observed in each segment*. A polynomial regression is performed at each segment of length s. The resulting trend, $Y_i^s(k)$, is then subtracted from the cumulative series, thereby obtaining "decorrelated" fluctuations:

$$F_i^2(s, v) = \frac{1}{s} \sum_{k=1}^{s} \left\{ Y_i[(v-1)s + k] - Y_i^s(k) \right\}^2, \qquad (9)$$

where $v = 1, 2, \ldots, N_s$ is the index of the segment.

(vi) *Calculating RMS fluctuation*. The root-mean-square (RMS) fluctuation is calculated for each and every segment:

$$F_i(s) = \sqrt{\frac{1}{N_s} \sum_{v=1}^{N_s} F_i^2(s, v)}. \qquad (10)$$

(vii) *Repeating for different scales*. Steps (iii)–(v) are repeated for different values of s, which correspond to different scales.

(viii) *Constructing the dependence and estimating the scale factor*. The function $F(s)$ is plotted on a logarithmic scale. In the event that the time series exhibits a self-similar structure, the aforementioned dependence will manifest as a straight line:

$$F_i(s) \sim s^{\mu_{\Delta f}^i}. \qquad (11)$$

The degree exponent $\mu_{\Delta f}^i$ (scale factor) is estimated by calculating the slope of the line on a logarithmic scale.

It should be noted that filtering introduces a correlation between neighboring samples of a signal, for example through convolution in the case of a FIR filter. Consequently, the inclusion of exceedingly narrow window sizes within the fitting range of the fluctuation function may result in the overestimation of temporal correlations [4]. The impact of a specific filter on the DFA scaling factor can be approximated through the use of white noise signals, which are expected to yield a μ value of 0.5. The algorithm is the following:

(1) One thousand white noise signals are generated.

(2) The requisite FIR filter is then applied to each signal.

(3) Subsequently, the amplitude envelopes of the filtered signals are extracted.

(4) A DFA is conducted for each signal, with all fluctuation functions subsequently averaged.

(5) The time windows for which the fluctuation function is approximately equal to 0.5 are estimated.

Table I specifies the extent of the window for each frequency range in which the filter influence is deemed to be insignificant.

The DFA scaling factor was calculated using the Neurophysiological Biomarker Toolbox software (NBT) [46].

E. Statistical testing

A statistical analysis of brain cortical activity in the spatial and frequency domains was conducted at the subject level for both time-averaged ERSPs ($w_{\Delta f}^i$) and the scaling factors ($\mu_{\Delta f}^i$) calculated for each ith EEG channel and five frequency ranges depending on the frequency of stimulation f_{IPS}. The statistical significance of the contrasts between conditions (control group and patients with diagnosed epilepsy) was evaluated using the permutation test with cluster-corrected multiple comparisons [47].

A statistic (t-statistic for independent samples) was calculated for each data point for the studied dataset. Subsequently, the sample elements were repeatedly shuffled between the conditions in order to create a set of potential data distributions that were consistent with the null hypothesis. Thereafter, the t-statistic was recalculated for each permutation. At each stage of the process, both the original dataset and each generated permutation were examined to identify clusters of adjacent points where the test statistic exceeded a specified significance threshold. For each cluster, the cluster statistic was calculated as the sum of the t-statistic values within the cluster. The value of the maximum statistic was then stored in order to construct an empirical distribution. The significance of clusters in the real data was determined by comparing the cluster statistic to the empirical distribution of the maximum cluster statistic derived from permutations. This allows us to ascertain the probability of observing such a cluster when the null hypothesis is true. Consequently, the issue of multiple comparisons was addressed by regulating the probability of false positive clusters, rather than that of individual data points. This method effectively reduces the number of false positives that result from multiple comparisons, it does not require the assumption of data normality, and it accounts for the spatial dependence between data points, which is of particular importance when analyzing EEG recordings.

Data points with $p < 0.01$ were grouped into separate positive and negative clusters. The minimum number of neighboring data points required to form a cluster was one. Such a minimal cluster size combined with a higher significance level threshold ($p < 0.01$) was chosen to ensure that statistical testing remained sensitive to local differences between groups [48]. A relatively small number of EEG channels (only 25) was used in our study. With a larger number of channels, neighboring points are more likely to have correlated signals, facilitating the formation of clusters. With fewer channels, the spatial density of the data is lower, which may result in significant effects localized in individual sensors not being included in the formed clusters. Using a minimum cluster size of one helps to overcome this limitation. A cluster was considered significant if its p-value was less than 0.025. A total of 1000 permutations were performed.

The analysis was conducted using MATLAB software with the Fieldtrip toolbox [41].

F. ML-based classifiers

Two distinct classifier types were investigated: one employing ERSP ($w_{\Delta f}^i$) values and another utilizing scaling factor ($\mu_{\Delta f}^i$) values. Both classifier types were implemented in two distinct variants.

The first variant of each classifier was trained using a feature set encompassing all $w^i_{\Delta f}$ or $\mu^i_{\Delta f}$ values across 25 EEG channels, 9 IPS frequencies, and 5 frequency bands (comprising the 4 standard frequency bands and stimulation frequency range), resulting in a total of 1125 features. To mitigate the dimensionality of the feature space, principal component analysis (PCA) was employed [49]. Determining the optimal number of principal components (PCs) with high explanatory power in relation to the original data variance is crucial in PCA. We implemented the following algorithm: the data were decomposed into several PCs, a threshold of explained variance was set to 85%, and then the minimum number of components that can explain a sufficiently high variance were selected. The resulting number of features was 15 for ERSP w and 46 for DFA scaling factor μ.

The second variant of each classifier was trained using only features exhibiting statistically significant differences between conditions, yielding 132 features for the ERSP-based classifier and 36 features for the DFA-based classifier.

A Support Vector Machine (SVM) classifier with a Linear Kernel was employed for training. This method has demonstrated effectiveness in EEG data analysis, including epilepsy diagnostics [50–53]. Linear SVM aims to identify an optimal hyperplane that effectively separates two classes in feature space, maximizing the margin between data points from each class. This approach enhances the model's robustness to noise and improves generalization capacity. A regularization parameter, denoted as R, acts as a hyperparameter, balancing the maximization of the margin and minimization of classification error to mitigate overfitting. The GridSearch method was employed to optimize this hyperparameter. Hyperparameter optimization aimed to maximize the F1-score [54].

ML model performance was assessed through k-fold cross-validation. Data from all subjects within the same group (patients or controls) were partitioned into $k = 10$ subsets. The model was trained on $k - 1$ subsets and evaluated on the remaining subset. This process was repeated five times.

To evaluate ML model quality, the following metrics were computed based on the number of true positives (TPs), true negatives (TNs), false positives (FPs), and false negatives (FNs):

Accuracy. The proportion of correct answers of an algorithm:

$$\text{Accuracy} = \frac{\text{TP+TN}}{\text{TP+TN+FP+FN}}. \tag{12}$$

Recall. The proportion of correctly found positive objects among all objects of positive class:

$$\text{Recall} = \frac{\text{TP}}{\text{TP+FN}}. \tag{13}$$

Precision. The proportion of correctly predicted positive objects among all objects predicted as a positive class:

$$\text{Precision} = \frac{\text{TP}}{\text{TP+FP}}. \tag{14}$$

F1-score. Harmonic mean between recall and accuracy:

$$\text{F1-score} = 2 \times \frac{\text{Precision} \times \text{Recall}}{\text{Precision+Recall}}. \tag{15}$$

G. Explainable ML technique to identify the features importance

The Boruta method [55] was employed to identify the most salient features for classification. This method operates by comparing original features to their corresponding "shadow features," which are generated through random shuffling of the original feature values. Features exhibiting minimal divergence from their shadow counterparts are deemed inconsequential for the model's predictive performance. The procedure involves the following steps:

(i) *Shadow Feature Creation:* Random combinations of original feature values are generated to create new features, which are appended to the dataset. These newly generated features are designated as "shadow features."

(ii) *Feature Importance Assessment:* The model is trained on the augmented dataset. For each feature (original and shadow), an importance value is calculated based on its influence on predicting the target variable. Feature importance is quantified by the reduction in classification accuracy resulting from its exclusion from the model.

(iii) *Feature Significance Determination:* The relative importance of each original feature is compared against the maximum importance of its associated shadow features. A feature is considered significant if its relative importance demonstrably exceeds that of any corresponding shadow features.

(iv) *Iterative Feature Elimination:* Unimportant features are systematically eliminated from the training dataset. This process is repeated iteratively until either a predefined number of iterations is reached or all features have been assigned an importance score.

III. RESULTS

A. Results of clustering analysis for ERSP

ERSPs ($w^i_{\Delta f}$) in the IPS frequency band, as well as in the δ-, θ-, α-, and β-frequency bands, were compared between healthy controls and patients with diagnosed epilepsy for each of the 9 IPS frequencies.

We considered statistically significant clusters observed in all ERSP comparisons across all investigated frequency bands and IPS frequencies. A comprehensive overview of these findings is presented in Table II, which lists all statistically significant clusters for all ERSP comparisons. Detailed illustrations of these clusters are shown in the Supplemental Material [56]. Figures 6–10 in the Supplemental Material show the statistically significant differences found after statistical analysis of the ERSP between the two experimental conditions: control group and patients with confirmed epilepsy. All EEG channels showing statistically significant differences between experimental conditions were grouped into positive and negative clusters, and marked with white circles. In positive clusters, the ERSP values are higher in the control group.

It is known that in the cluster permutation test, the precise localization of the effect is difficult—cluster boundaries may be unreliable due to the fact that a statistically significant effect is not guaranteed to be present in every data point within the cluster [57]. Therefore, the results should be interpreted

TABLE II. EEG channels in which ERSP ($w_{\Delta f}^i$) shows significant differences between conditions: controls and patients. "+" or "−" denotes positive (controls > patients) or negative (controls < patients) difference. Individual clusters are grouped in parentheses.

IPS frequency (Hz)	IPS band	δ-band	θ-band	α-band	β-band
1	"+" (T7, F9, T9)	"+" (T7, F9)			"+" (F8, T8)
3	"+" (F7, F9)	"+" (F7, T7, F9, T9), "+" (Fp2, F10)	"+" (Fp1, Fp2, F8, F9, T9, F10), "+" (O1, O2)	"−" (P7, T9, P9)	"+" (T8, P8)
8	"+" (O1, O2)	"+" (F7, F3, F9, T9), "+" (F8, F10, T10)	"+" (F8, F10)	"−" (T10, P10)	"+" (T7, T9)
10		"+" (F7, T7, F9)			"+" (F8, T8)
15	"+" (T7, F9, T9)	"+" (F3, Fz)		"−" (Fz, Cz, Pz)	"+" (F8, T8)
18	"+" (P7, O1)	"+" (Fp1, Fp2, Fz, F4)		"−" (Fz, Cz), "−" (P8, P10)	"+" (F8, T8)
20	"+" (F8, T8, P4, P8, F10, T10), "+" (T7, F9, P9)	"+" (Fp2, F3, Fz, T7)		"−" (Cz, Pz)	"+" (F8, T8, P8, F10)
25	"+" (Fp1, Fp2, F7, Fz, F8, T7, T8, P3, Pz, P4, O1, O2, F9, T9, F10, T10)	"+" (F3, Fz)	"+" (Fp2, F8, F10)	"−" (Cz, Pz)	"+" (O1, O2), "+" (T7, T9), "+" (FP1, FP2)
30	"+" (T8, Pz, P4, O1, O2, T10, P10) "+" (F7, T7)	"+" (T1, T9)		"−" (P8, T10, P10)	"+" (O1, O2)

with caution, and it is important to clarify the meaning of "statistically significant cluster." In our paper, statistically significant cluster is defined as a group of neighboring data point (channel, frequency) pairs for which the cluster statistics exceeds a given threshold (cluster permutation test shows that there is a significant effect of the condition). In this case, the localization of the cluster is defined within the considered frequency range (f_{IPS}, δ-, θ-, α-, and β-band) and the brain region identified during statistical testing.

Let us consider the detailed results separately for each investigated frequency range.

Comparison of ERSP in the IPS frequency band showed the following results. At IPS frequency of 1 Hz, the permutation test revealed one positive cluster with $p = 0.002$, which included the left temporal and frontal EEG channels. At an IPS frequency of 3 Hz, a positive cluster was observed in the left frontal region with $p < 0.001$. At an IPS frequency of 8 Hz, a positive cluster ($p = 0.006$) was detected in the occipital brain region. At an IPS frequency of 15 Hz, we observed a positive cluster with $p = 0.002$ in the left temporal and frontal brain regions. At an IPS frequency of 18 Hz, a positive cluster ($p < 0.001$) was found, which included EEG channels of the left parietal and occipital regions. At an IPS frequency of 20 Hz, the statistical test revealed a positive cluster with $p < 0.001$, which included EEG channels from parietal, temporal, and frontal brain regions. At an IPS frequency of 25 Hz, an extensive positive cluster was detected ($p < 0.001$), which included the majority of EEG channels. At an IPS frequency of 30 Hz, we found a positive cluster with $p = 0.002$ in occipital and temporal brain regions.

Comparison of ERSP in the δ-band showed the following results. At an IPS frequency of 1 Hz, a positive cluster was detected in the left temporal and frontal brain regions ($p < 0.001$). At an IPS frequency of 3 Hz, a positive cluster ($p < 0.001$) included EEG channels of the frontal and left temporal regions. At an IPS frequency of 8 Hz, the permuta-

tion test revealed a positive cluster with $p = 0.003$ involving channels of frontal and temporal brain regions in both the right and left hemispheres. At an IPS frequency of 10 Hz, we found a positive cluster ($p = 0.002$) in the left frontal and temporal brain regions. At an IPS frequency of 15 Hz, a positive cluster with $p < 0.001$ included EEG channels in the frontal brain region. A positive cluster at an IPS frequency of 18 Hz ($p = 0.002$) also included EEG channels of the frontal brain region. A positive cluster at an IPS frequency of 20 Hz with $p < 0.001$ included EEG channels of both frontal and left parietal regions. At an IPS frequency of 25 Hz, we found a positive cluster with $p < 0.001$ in the frontal brain region. At an IPS frequency of 30 Hz, a positive cluster ($p = 0.002$) was detected in the left temporal brain region.

Comparison of ERSP in the θ-band showed the following results. At an IPS frequency of 3 Hz, a positive cluster was identified with $p = 0.02$, which included EEG channels of occipital, frontal, and right temporal brain regions. At an IPS frequency of 8 Hz, we identified a positive cluster ($p = 0.02$) in the right frontal brain region. At an IPS frequency of 25 Hz, a positive cluster ($p = 0.04$) was detected also in the right frontal region.

Comparison of ERSP in the α-band showed the following results. At an IPS frequency of 3 Hz, the permutation test revealed a negative cluster with $p = 0.04$ in the left temporal and parietal brain regions. At an IPS frequency of 8 Hz, a negative cluster ($p = 0.04$) was detected in the right temporal and parietal brain regions. At an IPS frequency of 15 Hz, we detected a negative cluster with $p = 0.01$ in the central brain region. A negative cluster at an IPS frequency of 18 Hz ($p = 0.002$) included EEG channels of the right parietal brain region. At an IPS frequency of 20 Hz, a negative cluster with $p = 0.04$ was detected in the central brain region. At an IPS frequency of 25 Hz, a negative cluster ($p = 0.02$) was detected also in the central region. At an IPS frequency of 30 Hz, a negative cluster ($p = 0.003$) was detected in the right temporal and parietal brain regions.

TABLE III. EEG channels in which scaling factor ($\mu^i_{\Delta f}$) shows significant differences between conditions: controls and patients. "+" or "−" denotes positive (controls > patients) or negative (controls < patients) difference. Individual clusters are grouped in parentheses.

IPS frequency (Hz)	IPS band	δ-band	θ-band	α-band	β-band
1			"−" (O1, O2, P10)		"+" (P7)
3				"−" (T10)	
8	"−" (C4)		"−" (P10)	"−" (C4)	
10		"−" (C4, T8)	"−" (Pz)		
15			"−" (C4, P4)	"−" (Cz)	"+" (O1)
18	"+" (O1)		"−" (C4)	"−" (P9)	"+" (O1, O2)
20	"+" (P10)	"−" (P8)			"+" (O1), "+" (P10)
25	"+" (O1, O2)		"−" (P8)	"−" (F9)	"+" (O1)
30	"+" (Fp1, F7)		"−" (C3, Cz)	"−" (F3, C3, P3)	"+" (Fp2)

Comparison of ERSP in the β-band showed the following results. At an IPS frequency of 1 Hz, we found a positive cluster with $p = 0.01$, which included EEG channels of the right temporal and frontal brain regions. At an IPS frequency of 3 Hz, a positive cluster ($p = 0.01$) was located in the right temporal and parietal brain regions. A positive cluster ($p = 0.02$) was located in the left temporal brain region at an IPS frequency of 8 Hz. In the right temporal brain region, clusters were found at IPS frequencies of 10 Hz ($p = 0.04$), 15 Hz ($p = 0.008$), and 18 Hz ($p = 0.004$). At an IPS frequency of 20 Hz, the permutation test revealed a positive cluster with $p < 0.001$ in the right frontal, temporal, and parietal brain regions. At an IPS frequency of 25 Hz, we found a positive cluster ($p = 0.02$) involving channels of frontal, occipital, and left parietal brain regions. A positive cluster was detected in the occipital brain region with $p < 0.001$ at an IPS frequency of 30 Hz.

B. Results of clustering analysis for DFA

Scaling factors ($\mu^i_{\Delta f}$) in the IPS frequency band, as well as in the δ-, θ-, α-, and β-frequency bands, were compared between healthy controls and patients with diagnosed epilepsy for each of the 9 IPS frequencies.

We considered statistically significant clusters observed in all scaling factor ($\mu^i_{\Delta f}$) comparisons across all investigated frequency bands and IPS frequencies. A comprehensive overview of these findings is presented in Table III, which lists all statistically significant clusters for all scaling factor comparisons. Detailed illustrations of these clusters are shown in the Supplemental Material [56]. Figures 1–5 in the Supplemental Material show the statistically significant differences found after statistical analysis of the DFA scaling factor between the two experimental conditions: control group and patients with confirmed epilepsy. All EEG channels showing statistically significant differences between experimental conditions were grouped into positive and negative clusters, and marked with white circles. In positive clusters, the DFA scaling factor values are higher in the control group. Let us consider the detailed results separately for each investigated frequency range.

Comparison of scaling factor ($\mu^i_{\Delta f}$) in the band of stimulation frequency showed the following results. At an IPS frequency of 8 Hz, the permutation test revealed a negative cluster with $p = 0.002$, which included the central EEG chan-

nel C4. At an IPS frequency of 18 Hz, a positive cluster was observed in the occipital region with $p < 0.005$. At an IPS frequency of 20 Hz, a positive cluster ($p = 0.02$) was detected in the right parietal region of the brain. At an IPS frequency of 25 Hz, we observed a positive cluster with $p < 0.001$ in the occipital brain region. At an IPS frequency of 30 Hz, a positive cluster ($p = 0.04$) was detected, which included EEG channels of the frontal region.

Comparison of scaling factor ($\mu^i_{\Delta f}$) in the δ-band showed the following results. At an IPS frequency of 10 Hz, a negative cluster was detected in the right temporal and central brain regions ($p < 0.01$). At an IPS frequency of 20 Hz, a negative cluster ($p = 0.009$) included EEG channels of the left parietal region.

Comparison of scaling factor ($\mu^i_{\Delta f}$) in the θ-band showed the following results. At an IPS frequency of 1 Hz, a negative cluster was identified with $p = 0.01$, which included EEG channels of occipital and right parietal brain regions. At an IPS frequency of 8 Hz, we identified a negative cluster ($p < 0.001$) in the right parietal brain region. In the central parietal region, a negative cluster ($p = 0.01$) was detected at an IPS frequency of 10 Hz. In the right central and parietal brain regions, negative clusters were detected at IPS frequencies of 15 Hz ($p = 0.02$) and 18 Hz ($p = 0.04$). At an IPS frequency of 25 Hz, we detected a negative cluster with $p = 0.03$ in the right parietal brain region. At an IPS frequency of 30 Hz, the permutation test revealed a negative cluster ($p = 0.03$) in the central brain region.

Comparison of scaling factor ($\mu^i_{\Delta f}$) in the α-band showed the following results. At an IPS frequency of 3 Hz, the permutation test revealed a negative cluster with $p = 0.008$ in the right temporal brain region. At IPS frequencies of 8 Hz ($p = 0.002$) and 15 Hz ($p = 0.03$), negative clusters were detected in the central brain region. The negative cluster at an IPS frequency of 18 Hz ($p = 0.02$) included EEG channels of the left parietal brain region. At an IPS frequency of 25 Hz, a negative cluster with $p = 0.03$ was found in the left frontal brain region. At an IPS frequency of 30 Hz, a negative cluster ($p = 0.02$) was detected in the left frontal, central, and parietal brain regions.

Comparison of scaling factor ($\mu^i_{\Delta f}$) in the β-band showed the following results. At an IPS frequency of 1 Hz, we found a positive cluster with $p = 0.002$, which included EEG channels of the left parietal brain region. At an IPS frequency of 15 Hz, a positive cluster ($p = 0.003$) was located in the
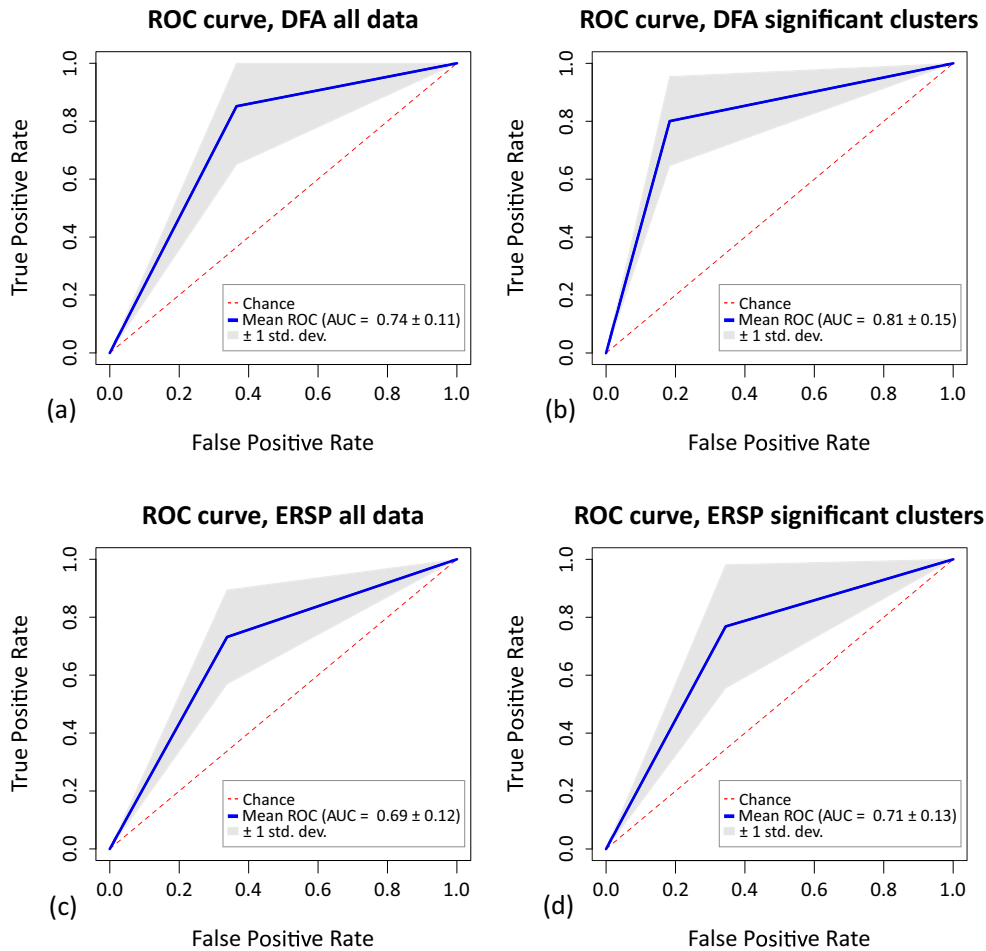
FIG. 3. Receiver operating characteristic (ROC-curves) for SVM classifiers: (a) all values of DFA scaling factors $\mu^i_{\Delta f}$ are used as features; (b) values of DFA scaling factors $\mu^i_{\Delta f}$ from statistically significant clusters are used as features; (c) all values of ERSP $w^i_{\Delta f}$ are used as features; (d) values of ERSP $w^i_{\Delta f}$ from statistically significant clusters are used as features.

occipital brain region. A positive cluster ($p < 0.001$) at an IPS frequency of 18 Hz was also located in the occipital region of the brain. In the occipital and right parietal brain regions, a cluster was detected at an IPS frequency of 20 Hz ($p = 0.006$). At an IPS frequency of 25 Hz, the permutation test revealed a positive cluster with $p = 0.01$ in the occipital brain region. At an IPS frequency of 30 Hz, we detected a positive cluster ($p = 0.02$) involving channels of the frontal brain region.

C. Results of classification for ERSP-based classifier and DFA-based classifier

Initially, two distinct classifiers were trained for the first variant (see Sec. II F). The first classifier employed all ERSP values ($w^i_{\Delta f}$) as predictors. These values were calculated during photic stimulation across 25 EEG channels, 9 IPS frequencies, and 5 frequency ranges, yielding 1125 features in total. PCA reduced this dimensionality to 15 features. The second classifier utilized scaling factors ($\mu^i_{\Delta f}$) derived from DFA, also encompassing 1125 initial features subsequently reduced to 46 by PCA. Both classifiers aimed to discriminate between patients and healthy controls.

The classification performance was significantly improved when using the DFA scaling factors ($\mu^i_{\Delta f}$) as predictors compared to the ERSP values ($w^i_{\Delta f}$). This superiority was observed across all metrics, as demonstrated by the following F1-scores: F1-score$_\mu = 0.78$ for the DFA-based classifier, and F1-score$_w = 0.7$ for the ERSP-based classifier. Furthermore, the DFA-based classifier achieved a higher accuracy (0.76 versus 0.67), precision (0.71 versus 0.65), and recall (0.88 versus 0.76) compared to the ERSP-based classifier. These findings are illustrated by the Receiver Operating Characteristic (ROC) curves in Fig. 3 [panels (a) and (c) for DFA-based and ERSP-based classifiers, respectively] and summarized in Table IV.

To assess the statistical significance of the achieved classification accuracy, a binomial test was conducted to determine if it exceeded the no information rate (NIR). NIR represents the baseline accuracy obtained by simply assigning all test samples to the most prevalent class in the dataset. The *p*-value (Acc > NIR) presented in Table IV indicates the probability of observing the same or higher accuracy as the model performing by chance, assuming the model's predictions are essentially random (i.e., equivalent to the NIR). This *p*-value corresponds to a hypothesis test where the null hypothesis

TABLE IV. F1-score, accuracy, precision, and recall for all classifiers trained on different types of input data

	All data		Significant clusters	
	ERSP, $w^i_{\Delta f}$	DFA, $\mu^i_{\Delta f}$	ERSP, $w^i_{\Delta f}$	DFA, $\mu^i_{\Delta f}$
F1-score	0.7	0.78	0.75	0.83
Accuracy	0.67	0.76	0.7	0.82
Precision	0.65	0.71	0.65	0.78
Recall	0.76	0.88	0.88	0.88
p-value (Acc > NIR)	0.02	0.001	0.01	0.00009

(H_0) states that the model accuracy is not significantly better than the NIR, while the alternative hypothesis (H_1) posits that the model's accuracy is significantly higher than the NIR. The statistical testing was performed using the standard model quality assessment tools available in the caret library for R [58].

Two additional classifiers, representing the second variant, were subsequently trained (see Sec. II F). The first classifier utilized ERSP values ($w^i_{\Delta f}$) calculated for EEG channels identified as statistically significant clusters, resulting in a total of 132 features (see Sec. III A). The second classifier employed scaling factors ($\mu^i_{\Delta f}$) derived from statistically significant clusters, yielding a total of 36 features (see Sec. III B).

The results revealed two key findings.

(i) *Improved performance with cluster-based feature selection*. Classifiers trained on statistically significant clusters demonstrated improved performance compared to those trained on the entire feature set. Specifically, the ERSP-based classifier utilizing ERSP values ($w^i_{\Delta f}$) from significant clusters exhibited an increase in F1-score (0.75 versus 0.7), accuracy (0.7 versus 0.67), and recall (0.88 versus 0.76), while maintaining the same precision. Similarly, the DFA-based classifier using scaling factor values ($\mu^i_{\Delta f}$) from significant clusters showed improvements in the F1-score (0.83 versus 0.78), accuracy (0.82 versus 0.76), and precision (0.78 versus 0.71) with no change in recall.

(ii) *Superiority of DFA-based classifiers*. Consistent with the initial findings, the DFA-based classifier utilizing scaling factors ($\mu^i_{\Delta f}$) as predictors (F1-score = 0.83) demonstrated significantly better classification performance compared to the ERSP-based classifier (F1-score = 0.75). This trend was also observed in accuracy (0.82 versus 0.7) and precision (0.78 versus 0.65), while recall remained comparable. These results are further illustrated in Fig. 3 [panels (b) and (d)] and summarized in Table IV.

Table IV reveals that all four classifiers demonstrate statistically significant accuracy compared to a random classifier. However, a consistent trend emerges: classifiers utilizing the scaling factor $\mu^i_{\Delta f}$ achieve higher F1-scores than their ERSP-based counterparts. Notably, the classifier employing $\mu^i_{\Delta f}$ and trained on significant clusters attains an F1-score exceeding 0.8, making it a promising candidate for practical applications due to its superior performance.

These findings highlight the potential benefits of using statistically significant clusters for feature selection, improving classification performance. Moreover, the consistent superiority of the DFA-based classifier reinforces the value of DFA-derived features in characterizing brain dynamics related to neurological conditions.

To identify the most influential features for classification, we employed the Boruta method (see Sec. II G). Figure 4 presents a box-plot diagram ranking features by their importance level, alongside a topogram visualization of the most salient features.

Figure 4, panels (a) and (c), presents a box-plot diagram illustrating the distribution of the z-score of the features, calculated as the ratio of the average decrease in classification accuracy resulting from the random permutation of features to its standard deviation. The figure shows only those features whose z-score is consistently higher than that of the shadow features.

Analysis of the feature importance reveals distinct patterns between the DFA-based classifier and the ERSP-based classifier [cf. panels (a) and (c) in Fig. 4]. For the DFA-based classifier, which distinguishes patients with epilepsy, the most important features are associated with long-range temporal correlations in the central brain area (EEG channel C4) within the α-band and in the occipital region within the β-band [see Fig. 4, panel (b); white circles indicate the most important features for classification]. Conversely, the ERSP-based classifier identifies ERSP values at high stimulation frequencies in the parietal, frontal, and right temporal brain areas as the most influential features for classifying patients with epilepsy [see Fig. 4, panel (d); white circles indicate the most important features for classification].

This disparity in feature importance underscores the distinct information captured by DFA scaling factors ($\mu^i_{\Delta f}$) and ERSP values ($w^i_{\Delta f}$), emphasizing the potential of DFA as a valuable tool for understanding brain dynamics in epilepsy.

Figure 5 presents a visualization of significant brain responses across various photic stimulation frequencies for both DFA and ERSP analyses, revealing variations in response patterns across frequency bands and brain regions. To provide a more comprehensive visualization of the significant features, the scalp electrodes were grouped into six distinct regions: frontal, central, left temporal, right temporal, parietal, and occipital [see Fig. 5(a)]. Figures 5(b) and 5(c) further depict the visualization of significant features for both the DFA scaling factors $\mu^i_{\Delta f}$ [Fig. 5(b)] and the ERSP $w^i_{\Delta f}$ values [Fig. 5(c)]. The y-axis represents the IPS frequencies, while the x-axis indicates the frequency ranges within which brain responses were considered significant for classification. Colored segments highlight brain responses to specific IPS frequencies within particular frequency ranges and brain regions, indicating their importance for classification. The symbols "−" and "+" denote negative and positive clusters, respectively. In positive clusters, the values of the scaling factors $\mu^i_{\Delta f}$ or ERSP $w^i_{\Delta f}$ were higher in the control group.

So, Fig. 5(b) highlights the features deemed crucial for classification when utilizing the DFA scaling factor $\mu^i_{\Delta f}$. Within the δ-band (response frequencies 1 and 3 Hz), a brain response is observed at IPS frequencies of 10, 20, and 30 Hz in the central and parietal areas. Similarly, in the α-band (response frequencies 8 and 10 Hz), a brain response is detected at IPS frequencies of 3 and 8 Hz in the central and right temporal areas, at 18 Hz in the parietal area, and at 25 and 30 Hz in the left temporal, central, and frontal areas. Within
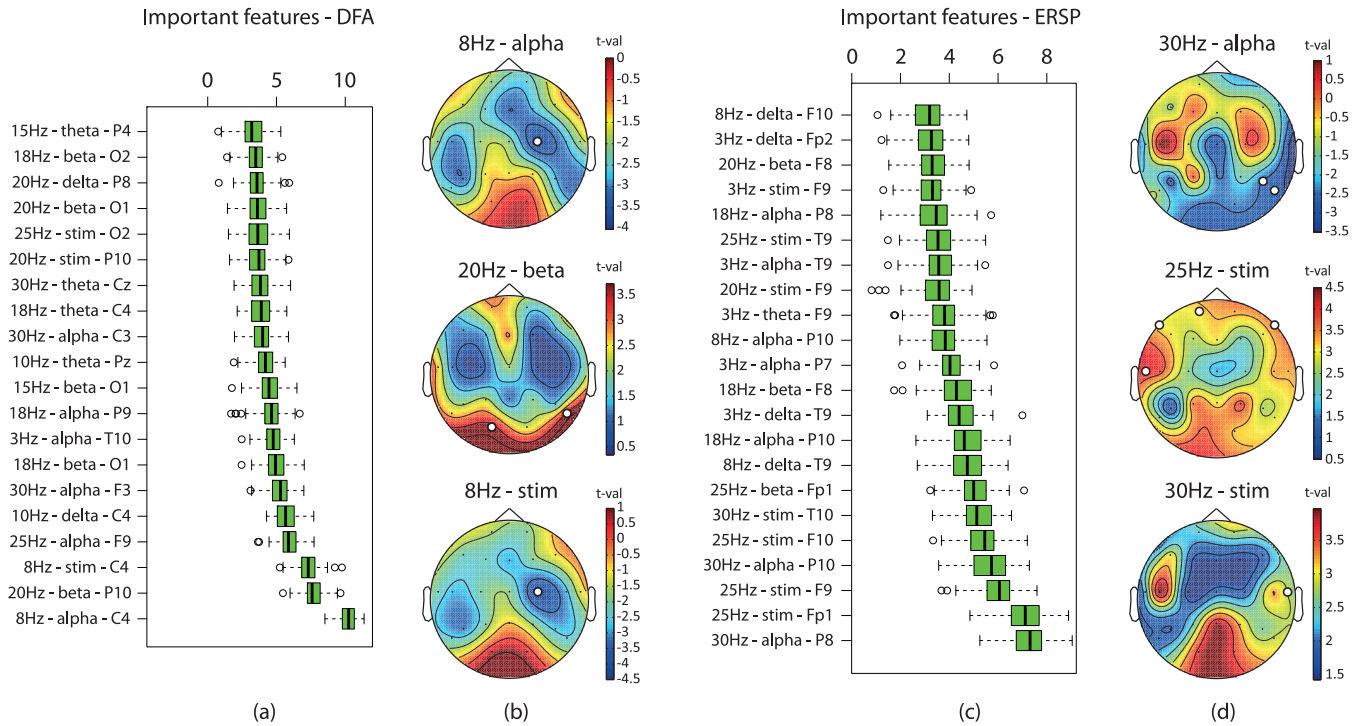
FIG. 4. Feature significance assessed with the Boruta method: (a) all significant features of scaling factors $\mu^i_{\Delta f}$; (b) visualization of the most important features of scaling factors $\mu^i_{\Delta f}$ on the head surface; (c) all significant features of ERSP $w^i_{\Delta f}$; (d) visualization of the most important features of ERSP $w^i_{\Delta f}$ on the head surface. Feature naming follows the following structure: "IPS frequency" – "frequency band"–"EEG channel"; "stim" stands for IPS frequency band. White circles indicate the most important features for classification.

the β-band (response frequencies 15, 18, 20, 25, and 30 Hz), a brain response is observed at IPS frequencies of 15, 18, 20, and 25 Hz, with a predominant presence in the occipital area and a partial presence in the parietal area.

Figure 5(c) illustrates the features critical for classification when employing ERSP values $w^i_{\Delta f}$. A brain response in the δ-band (response frequencies 1 and 3 Hz) was observed at IPS frequencies of 3 and 8 Hz in the left and right temporal areas. Additionally, an α-band (response frequencies 8 and 10 Hz) brain response was observed in the left temporal and parietal areas at IPS frequencies of 3 and 8 Hz. Stimulation frequencies of 18 and 30 Hz elicited an α-band brain response in the parietal area. In the β-band (response frequencies 15, 18, 20, 25, and 30 Hz), a brain response is observed at IPS frequencies of 18, 20, 25, and 30 Hz, primarily in the frontal area and to a lesser extent in the left and right temporal areas.

IV. DISCUSSION

A. Significant features of ERSP

Analysis of the brain response in the α-band (response frequencies of 8 and 10 Hz) at stimulation frequencies (f_{IPS}) of 3, 8, 18, and 30 Hz [see Fig. 5(c)] revealed a distinct pattern in parietal and left temporal areas. This can be interpreted as PD observed at the stimulation frequency, along with its harmonics and subharmonics. While this pattern is commonly encountered, researchers have noted that PD predominantly occurring at low (<6 Hz) or high (>25 Hz) IPS frequencies, as well as its spread beyond parietal and occipital areas, are generally considered indicators of brain dysfunction [59]. In

control subjects, PD is expected within the α-band or within the range of spontaneous activity in occipital regions [59]. Studies utilizing CWT analysis for investigating IPS rely heavily on the PD response in EEG, often focusing on the occipital area where PD is most pronounced [24,26]. However, some studies of pathological conditions, such as schizophrenia [60], suggest that PD-based differences between patients and controls can be identified in a wider area of the cortex, encompassing midfrontal and central regions.

The observed results present an intriguing pattern. Clusters identified at low and high frequencies exhibit a positive trend (i.e., higher PD in control subjects), while clusters in the α-band display a negative trend (i.e., lower PD in control subjects). This finding contrasts with that of some researchers who posit that PD should be elevated in patients with various neural disorders, with controls demonstrating only faint α-band PD, albeit lower than in patients [26]. Conversely, other studies have reported lower PD in patients with migraines, for instance [24]. Findings specific to epilepsy are ambiguous. For example, one study [25] suggested lower PD in patients, based on analysis of cerebral blood flow, which only partially correlates with EEG activity. It is generally accepted that seizure initiation involves a loss of inhibitory control, leading to increased excitability [7]. The magnitude of PD can be linked to cortical excitability and, therefore, considered a potential biomarker of epileptic conditions, although this has only been demonstrated for photosensitive epilepsy cases [61].

The observed findings appear to contradict some existing studies [7,61]. However, it is important to note that the
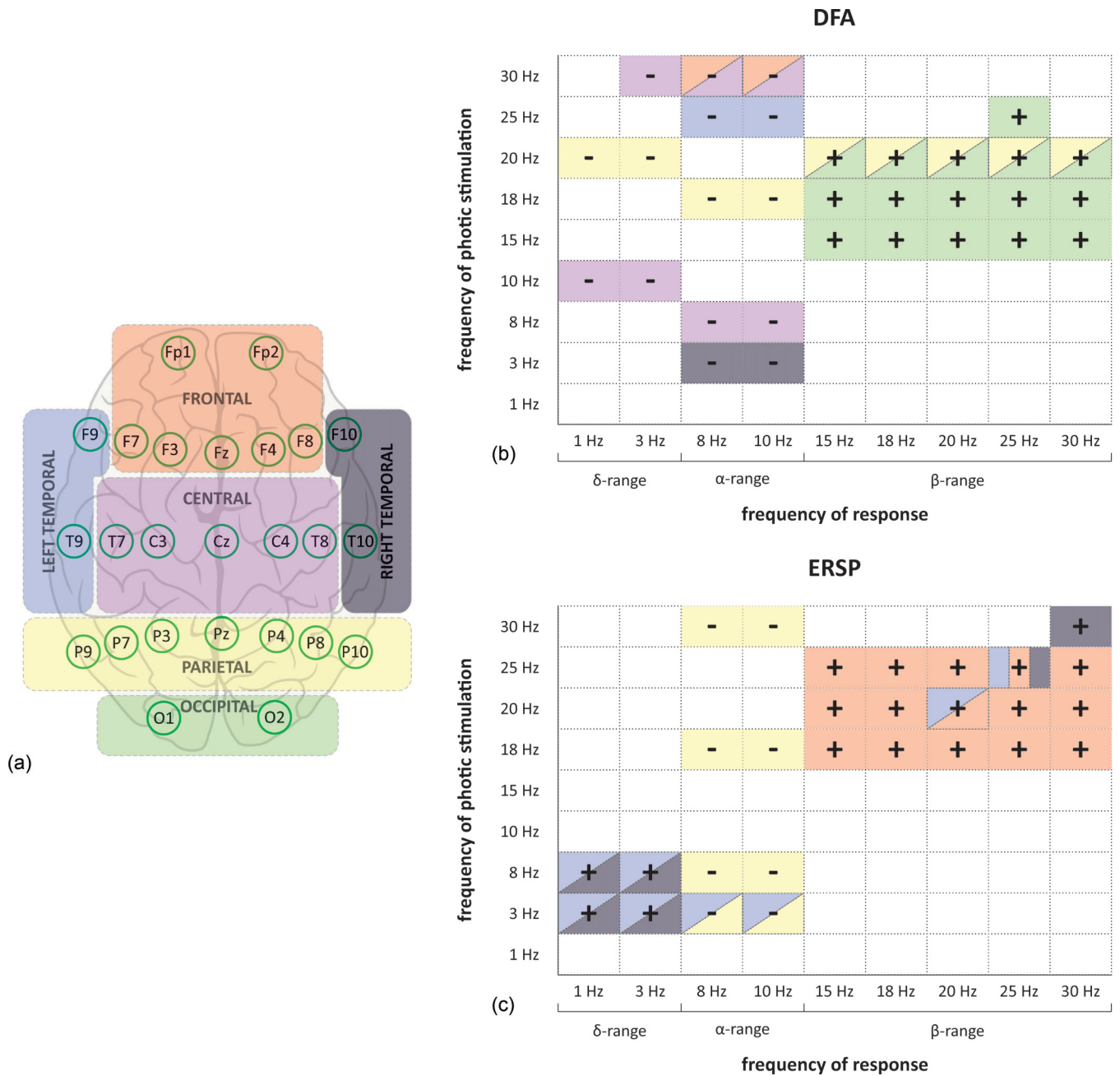
FIG. 5. Visual representation of significant features: (a) schematic of EEG channels segmentation into six regions: frontal (red), central (purple), left temporal (blue), right temporal (gray), parietal (yellow), and occipital (green); visualization of scaling factors $\mu^i_{\Delta f}$ (b) and ERSP $w^i_{\Delta f}$ (c) features significant for classification. A segment is colored if the brain response to certain IPS frequency in certain frequency range and brain region was deemed significant. The symbols "−" or "+" denote negative and positive clusters, respectively.

majority of these studies focus on *photosensitive* epilepsy, while the present work exclusively examines *nonphotosensitive* epilepsy. These two types of epilepsy are likely to differ in their underlying mechanisms, rendering some previously established results potentially irrelevant to the findings of the present study. For example, PD symmetry is a significant factor: asymmetrical responses suggest impairment located in one side of the brain, a common finding in focal epilepsy. The absence of asymmetrical response, as observed in our results, may indicate that the occipital cortex is not severely affected and visual pathways remain intact, consistent with the manifestation of nonphotosensitive epilepsy.

While the established mechanisms linking increased excitability to seizure initiation are difficult to refute, it is worthwhile to speculate about the nature of excitability itself. In general, decreased excitability is often encountered in patients exposed to antiepileptic drugs [62]. However, this cannot be the case in the present study, since epilepsy was drug-resistant in all patients and none of the patients were taking antiepileptic drugs at the time of clinical monitoring. Our findings indicate that patients exhibit decreased excitability in frontal and temporal areas, a pattern atypical for photosensitive epilepsy [59]. However, it is well known that excitability is dynamic [7]. For instance, cortical excitability can decrease

in the peri-ictal state following a seizure [63]. Therefore, we propose that nonphotosensitive epileptic patients may experience periods of heightened excitability, coinciding with seizure onset, while at other times excitability may be reduced, potentially even lower than in controls, as part of a compensatory mechanism.

B. Significant features of DFA

A notable discrepancy emerges when comparing cluster patterns generated by ERSP and DFA analyses. While ERSP and DFA clusters exhibit significant overlap in the α- and β-bands, including concordant patterns of positivity and negativity, they diverge considerably in the δ range. Notably, ERSP and DFA clusters in the δ range do not overlap in the "response frequency/IPS frequency" space.

Further differences arise in the spatial distribution of clusters on the scalp. For instance, ERSP clusters in the β-band are predominantly localized in frontal and, to a lesser extent, temporal areas. In contrast, DFA clusters in the β-band are exclusively confined to occipital and parietal regions. Similarly, DFA clusters in the α-band are broadly distributed across the cortex, whereas ERSP clusters in the α-band are primarily concentrated in parietal areas.

A direct comparison of ERSP and DFA features is challenging due to the ongoing debate surrounding the interpretation of the DFA exponent and the general presence of long-range temporal correlations in neuronal oscillations. Nonetheless, a prominent hypothesis posits that the brain operates in a critical state, and LRTC reflects this critical state dynamics [2,64]. Computational models have demonstrated that criticality in neuronal networks is associated with optimal information processing [65]. At the level of neuronal populations, criticality manifests as scale-free distributions of local field potential propagations, so-called neuronal avalanches [4].

It was shown that LRTC emerges only when networks produce critical neuronal avalanches, and this occurs when excitatory and inhibitory connectivities are balanced [8]. Importantly, these studies suggest a crucial functional role for LRTC: an optimal level of temporal structure in oscillations exists, and deviations from this optimum can lead to significant functional impairments [4,8]. This emphasis on excitatory-inhibitory balance aligns with existing models of epileptic seizure initiation [66,67].

Considering these findings, both ERSP and the DFA exponent may provide insights into EEG signal features related to excitatory and inhibitory control. However, given the superior classification performance of DFA-based classifiers, it is plausible that DFA features are more robust and potentially reflect aspects of EEG data missed by CWT-based analysis. We hypothesize that the presence of LRTC in epileptic EEG might be one such feature.

V. CONCLUSION

This study explored two distinct approaches for analyzing EEG data with brain response to intermittent photic stimula-

tion (IPS) in patients with nonphotosensitive focal epilepsy: classical spectral analysis using CWT, and the assessment of long-range temporal correlations using DFA. Both approaches employed features derived from 25 EEG channels, 9 stimulation frequencies, and 5 frequency bands encompassing potential brain responses. To compare feature characteristics between patients and healthy controls, cluster analysis was performed. Additionally, machine learning classifiers were trained on features from both approaches, considering two feature sets: all possible features reduced by principal component analysis and statistically significant features.

The results demonstrated superior performance of classifiers based on DFA features. Feature importance analysis in the machine learning classifiers revealed notable differences between the significant features identified by CWT and DFA. Specifically, DFA analysis did not reveal a "resonant" brain response at very low IPS frequencies, but for higher IPS frequencies the brain response shifted from frontal and temporal areas, as observed in CWT clusters, to parietal and occipital areas. Considering the superior performance of the DFA-based classifier, this observation suggests that LRTCs, as assessed through DFA, may offer novel insights into EEG responses to IPS in nonphotosensitive focal epilepsy.

The findings of this research hold significant value. The novel aspects of EEG revealed by DFA may provide support for existing theories regarding epileptic seizure emergence through mechanisms of excitatory-inhibitory control, as reflected in CWT spectra. However, the identified differences in DFA features suggest that they capture distinct and more relevant information, considering the results of machine learning classification. This information may be linked to changes in LRTCs, characteristic to epileptic EEG. These findings contribute to research on epilepsy and the role of LRTCs in neuronal oscillations more broadly.

The study also holds practical implications. IPS is commonly employed along with hyperventilation as an express diagnostic tool for photosensitive epilepsy. As we discussed in the Introduction, IPS aims to trigger a specific response in EEG, exclusive to photosensitive epilepsy. The rarity of photosensitive epilepsy among other cases makes IPS unsuitable for general diagnostic purposes. However, our findings demonstrate that IPS can effectively reveal important features even in nonphotosensitive cases using both CWT and DFA-based approaches. This potentially expands the clinical application of IPS, as appropriate analysis of EEG during IPS can reveal distinctions between epileptic patients and healthy controls. The combination of a common routine with an IPS session and described data analysis approach creates prospects for the development of a novel express diagnostic tool that requires no additional clinical procedures but extends the scope of applicability for a conventional IPS procedure.

[1] M. Paluš, Nonlinearity in normal human EEG: Cycles, temporal asymmetry, nonstationarity and randomness, not chaos, Biol. Cybern. **75**, 389 (1996).

[2] K. Linkenkaer-Hansen, V. V. Nikouline, J. M. Palva, and R. J. Ilmoniemi, Long-range temporal correlations and scaling behavior in human brain oscillations, J. Neurosci. **21**, 1370 (2001).

[3] C.-K. Peng, S. V. Buldyrev, S. Havlin, M. Simons, H. E. Stanley, and A. L. Goldberger, Mosaic organization of DNA nucleotides, Phys. Rev. E **49**, 1685 (1994).

[4] R. Hardstone, S.-S. Poil, G. Schiavone, R. Jansen, V. V. Nikulin, H. D. Mansvelder, and K. Linkenkaer-Hansen, Detrended fluctuation analysis: A scale-free view on neuronal oscillations, Front. Physiol. **3**, 450 (2012).

[5] D. Kasteleijn-Nolst Trenité, G. Rubboli, E. Hirsch, A. Martins da Silva, S. Seri, A. Wilkins, J. Parra, A. Covanis, M. Elia, G. Capovilla *et al.*, Methodology of photic stimulation revisited: Updated European algorithm for visual stimulation in the EEG laboratory, Epilepsia **53**, 16 (2012).

[6] F. Fylan, A. Edson, and G. Harding, Clinical significance of EEG abnormalities during photic stimulation in patients with photosensitive epilepsy, Epilepsia **40**, 370 (1999).

[7] R. Badawy, D. Freestone, A. Lai, and M. Cook, Epilepsy: Ever-changing states of cortical excitability, Neuroscience **222**, 89 (2012).

[8] S.-S. Poil, R. Hardstone, H. D. Mansvelder, and K. Linkenkaer-Hansen, Critical-state dynamics of avalanches and oscillations jointly emerge from balanced excitation/inhibition in neuronal networks, J. Neurosci. **32**, 9817 (2012).

[9] L. Berthouze, L. M. James, and S. F. Farmer, Human EEG shows long-range temporal correlations of oscillation amplitude in theta, alpha and beta bands across a wide age range, Clin. Neurophysiol. **121**, 1187 (2010).

[10] X. Bornas, M. Noguera, M. Balle, A. Morillas-Romero, B. Aguayo-Siquier, M. Tortella-Feliu, and J. Llabrés, Long-range temporal correlations in resting EEG, J. Psychophysiol. **27**, 60 (2013).

[11] M. Wairagkar, Y. Hayashi, and S. J. Nasuto, Dynamics of long-range temporal correlations in broadband EEG during different motor execution and imagery tasks, Front. Neurosci. **15**, 660032 (2021).

[12] G. Buzsaki, *Rhythms of the Brain* (Oxford University Press, Oxford, UK, 2006).

[13] J. B. Bassingthwaighte, L. S. Liebovitch, and B. J. West, *Fractal Physiology* (Springer, Berlin, 2013).

[14] B. J. He, J. M. Zempel, A. Z. Snyder, and M. E. Raichle, The temporal structures and functional significance of scale-free brain activity, Neuron **66**, 353 (2010).

[15] B. J. West, Fractal physiology and the fractional calculus: A perspective, Front. Physiol. **1**, 12 (2010).

[16] O. Sysoeva, V. Maximenko, A. Kuc, V. Voinova, O. Martynova, and A. Hramov, Abnormal spectral and scale-free properties of resting-state EEG in girls with Rett syndrome, Sci. Rep. **13**, 12932 (2023).

[17] K. Linkenkaer-Hansen, D. J. Smit, A. Barkil, T. E. van Beijsterveldt, A. B. Brussaard, D. I. Boomsma, A. van Ooyen, and E. J. de Geus, Genetic contributions to long-range temporal correlations in ongoing oscillations, J. Neurosci. **27**, 13882 (2007).

[18] D. J. Smit, E. J. de Geus, M. E. van de Nieuwenhuijzen, C. E. van Beijsterveldt, G. C. M. van Baal, H. D. Mansvelder, D. I. Boomsma, and K. Linkenkaer-Hansen, Scale-free modulation of resting-state neuronal oscillations reflects prolonged brain maturation in humans, J. Neurosci. **31**, 13128 (2011).

[19] S. Monto, S. Vanhatalo, M. D. Holmes, and J. M. Palva, Epileptogenic neocortical networks are revealed by abnormal temporal dynamics in seizure-free subdural EEG, Cereb. Cortex **17**, 1386 (2007).

[20] F. Hohlefeld, J. Huebl, C. Huchzermeyer, G.-H. Schneider, T. Schönecker, A. Kühn, G. Curio, and V. V. Nikulin, Long-range temporal correlations in the subthalamic nucleus of patients with Parkinson's disease, Eur. J. Neurosci. **36**, 2812 (2012).

[21] V. Padmanaban, S. Inati, A. Ksendzovsky, and K. Zaghloul, Clinical advances in photosensitive epilepsy, Brain Res. **1703**, 18 (2019).

[22] C. V. de Pémille, S. Rekik, H. Amiel, E. Meppiel, A. Richard, S. Masmoudi, N. Kubis, and P. Lozeron, Contribution of intermittent photic stimulation to routine EEG, Neurophysiol. Clin. **51**, 549 (2021).

[23] V. V. Lazarev, A. Pontes, and L. C. deAzevedo, EEG photic driving: Right-hemisphere reactivity deficit in childhood autism. A pilot study, Int. J. Psychophysiol. **71**, 177 (2009).

[24] M. Bjørk, K. Hagen, L. Stovner, and T. Sand, Photic EEG-driving responses related to ictal phases and trigger sensitivity in migraine: A longitudinal, controlled study, Cephalalgia **31**, 444 (2011).

[25] B. Diehl, S. R. Stodieck, R. R. Diehl, and E. B. Ringelstein, The photic driving EEG response and photoreactive cerebral blood flow in the posterior cerebral artery in controls and in patients with epilepsy, Electroencephalogr. Clin. Neurophysiol. **107**, 8 (1998).

[26] I. Svyatogor, O. Dick, A. Nozdrachev, and N. Guseva, Analysis of changes in EEG patterns in response to rhythmic photic stimulation under various disruptions of the functional state of the central nervous system, Hum. Physiol. **41**, 261 (2015).

[27] Y. Fogang, P. Gérard, V. De Pasqua, J.-L. Pepin, M. Ndiaye, D. Magis, and J. Schoenen, Analysis and clinical correlates of 20 Hz photic driving on routine EEG in migraine, Acta Neurol. Belg. **115**, 39 (2015).

[28] C. M. Childs and N. R. Washburn, Embedding domain knowledge for machine learning of complex material systems, MRS Commun. **9**, 806 (2019).

[29] D. Kerrigan, J. Hullman, and E. Bertini, A survey of domain knowledge elicitation in applied machine learning, Multimodal Technol. Interact. **5**, 73 (2021).

[30] V. A. Huynh-Thu, Y. Saeys, L. Wehenkel, and P. Geurts, Statistical interpretation of machine learning-based feature importance scores for biomarker discovery, Bioinformatics **28**, 1766 (2012).

[31] A. Kuc, S. Korchagin, V. A. Maksimenko, N. Shusharina, and A. E. Hramov, Combining statistical analysis and machine learning for EEG scalp topograms classification, Front. Syst. Neurosci. **15**, 716897 (2021).

[32] G. Casalicchio, C. Molnar, and B. Bischl, Visualizing the feature importance for black box models, in *Machine Learning and Knowledge Discovery in Databases: European Conference, ECML PKDD 2018, Dublin, Ireland, 2018, Proceedings, Part I 18* (Springer, Berlin, 2019), pp. 655–670.

[33] A. M. Musolf, E. R. Holzinger, J. D. Malley, and J. E. Bailey-Wilson, What makes a good prediction? feature importance

and beginning to open the black box of machine learning in genetics, Hum. Genet. **141**, 1515 (2022).

[34] A. B. Arrieta, N. Díaz-Rodríguez, J. Del Ser, A. Bennetot, S. Tabik, A. Barbado, S. García, S. Gil-López, D. Molina, R. Benjamins *et al.*, Explainable Artificial Intelligence (XAI): Concepts, taxonomies, opportunities and challenges toward responsible AI, Inf. Fusion **58**, 82 (2020).

[35] E. Tjoa and C. Guan, A survey on explainable artificial intelligence (XAI): Toward medical XAI, IEEE Trans. Neural Netw. Learn. Syst. **32**, 4793 (2020).

[36] S. Reddy, Explainability and artificial intelligence in medicine, Lancet Digital Health **4**, e214 (2022).

[37] D. Kasteleijn-Nolst Trenite, Photosensitivity and epilepsy, in *Clinical Electroencephalography*, edited by O. Mecarelli (Springer, Cham, 2019), pp. 487–495.

[38] M. Khazi, A. Kumar, and M. Vidya, Analysis of EEG using 10: 20 electrode system, Int. J. Innovative Res. Sci., Eng. Technol. **1**, 185 (2012).

[39] D. M. White and C. A. Van Cott, EEG artifacts in the intensive care unit setting, Am. J. Electroneurodiagnostic Technol. **50**, 8 (2010).

[40] J. Iriarte, E. Urrestarazu, M. Valencia, M. Alegre, A. Malanda, C. Viteri, and J. Artieda, Independent component analysis as a tool to eliminate artifacts in EEG: A quantitative study, J. Clin. Neurophysiol. **20**, 249 (2003).

[41] R. Oostenveld, P. Fries, E. Maris, and J.-M. Schoffelen, Fieldtrip: Open source software for advanced analysis of MEG, EEG, and invasive electrophysiological data, Comput. Intell. Neurosci. **2011**, 1 (2011).

[42] A. E. Hramov, A. A. Koronovskii, V. A. Makarov, A. N. Pavlov, and E. Sitnikova, *Wavelets in Neuroscience* (Springer, Berlin, 2015).

[43] R. T. Ogden, *Essential Wavelets for Statistical Applications and Data Analysis* (Birkhäuser, Boston, MA, 1997).

[44] C.-K. Peng, S. Havlin, H. E. Stanley, and A. L. Goldberger, Quantification of scaling exponents and crossover phenomena in nonstationary heartbeat time series, Chaos **5**, 82 (1995).

[45] F. R. Kschischang, *The Hilbert Transform* (University of Toronto, Toronto, ON, Canada, 2006).

[46] http://www.nbtwiki.net/

[47] E. Maris and R. Oostenveld, Nonparametric statistical testing of EEG-and MEG-data, J. Neurosci. Meth. **164**, 177 (2007).

[48] G. Huang and Z. Zhang, Improving sensitivity of cluster-based permutation test for EEG/MEG data, in *Proceedings of the 2017 8th International IEEE/EMBS Conference on Neural Engineering (NER)* (IEEE, Piscataway, NJ, 2017), pp. 9–12.

[49] R. Bro and A. K. Smilde, Principal component analysis, Anal. Meth. **6**, 2812 (2014).

[50] R. Panda, P. Khobragade, P. Jambhule, S. Jengthe, P. Pal, and T. Gandhi, Classification of EEG signal using wavelet transform and support vector machine for epileptic seizure diction, in *Proceedings of the 2010 International Conference on Systems in Medicine and Biology* (IEEE, Piscataway, NJ, 2010), pp. 405–408.

[51] N. Nicolaou and J. Georgiou, Detection of epileptic electroencephalogram based on permutation entropy and support vector machines, Expert Syst. Appl. **39**, 202 (2012).

[52] O. E. Karpov, V. V. Grubov, V. A. Maksimenko, S. A. Kurkin, N. M. Smirnov, N. P. Utyashev, D. A. Andrikov, N. N. Shusharina, and A. E. Hramov, Extreme value theory inspires explainable machine learning approach for seizure detection, Sci. Rep. **12**, 11474 (2022).

[53] O. E. Karpov, M. S. Khoymov, V. A. Maksimenko, V. V. Grubov, N. Utyashev, D. A. Andrikov, S. A. Kurkin, and A. E. Hramov, Evaluation of unsupervised anomaly detection techniques in labelling epileptic seizures on human EEG, Appl. Sci. **13**, 5655 (2023).

[54] C. Goutte and E. Gaussier, A probabilistic interpretation of precision, recall and f-score, with implication for evaluation, in *European Conference on Information Retrieval* (Springer, Berlin, 2005), pp. 345–359.

[55] M. B. Kursa and W. R. Rudnicki, Feature selection with the boruta package, J. Stat. Soft. **36**, 1 (2010).

[56] See Supplemental Material at http://link.aps.org/supplemental/10.1103/PRXLife.3.013005 for additional details statistically significant spatial clusters for different frequency ranges obtained by comparing DFA scaling factor and ERSP between controls and epileptic patients.

[57] J. Sassenhagen and D. Draschkow, Cluster-based permutation tests of MEG/EEG data do not establish significance of effect latency or location, Psychophysiology **56**, e13335 (2019).

[58] M. Kuhn, Building predictive models in R using the caret package, J. Stat. Soft. **28**, 1 (2008).

[59] L. Ponsen, Photic stimulation, Am. J. EEG Technol. **14**, 173 (1974).

[60] Y. Jin, C. Sandman, J. Wu, J. Bernat, and S. Potkin, Topographic analysis of EEG photic driving in normal and schizophrenic subjects, Clin. Electroencephalogr. **26**, 102 (1995).

[61] M. Vranic-Peters, P. O'Brien, U. Seneviratne, A. Reynolds, A. Lai, D. B. Grayden, M. J. Cook, and A. D. Peterson, Response to photic stimulation as a measure of cortical excitability in epilepsy patients, Front. Neurosci. **17**, 1308013 (2024).

[62] R. L. Macdonald and K. M. Kelly, Antiepileptic drug mechanisms of action, Epilepsia **36**, S2 (1995).

[63] R. Badawy, R. Macdonell, G. Jackson, and S. Berkovic, The peri-ictal state: Cortical excitability changes within 24 h of a seizure, Brain **132**, 1013 (2009).

[64] C. T. Kello, G. D. Brown, R. Ferrer-i Cancho, J. G. Holden, K. Linkenkaer-Hansen, T. Rhodes, and G. C. Van Orden, Scaling laws in cognitive sciences, Trends Cognit. Sci. **14**, 223 (2010).

[65] O. Kinouchi and M. Copelli, Optimal dynamical range of excitable networks at criticality, Nat. Phys. **2**, 348 (2006).

[66] A. Depaulis, M. Vergnes, and C. Marescaux, Endogenous control of epilepsy: The nigral inhibitory system, Prog. Neurobiol. **42**, 33 (1994).

[67] F. L. Da Silva, W. Blanes, S. N. Kalitzin, J. Parra, P. Suffczynski, and D. N. Velis, Epilepsies as dynamical diseases of brain systems: Basic models of the transition between normal and epileptic activity, Epilepsia **44**, 72 (2003).